Retrieval of Atmospheric Water Vapor Density With Fine Spatial Resolution Using Three-Dimensional Tomographic Inversion of Microwave Brightness Temperatures Measured by a Network of Scanning Compact Radiometers

Sharmila Padmanabhan, *Student Member, IEEE*, Steven C. Reising, *Senior Member, IEEE*, Jothiram Vivekanandan, and Flavio Iturbide-Sanchez, *Member, IEEE*

***Abstract*—Quantitative precipitation forecasting is currently limited by the paucity of observations on sufficiently fine temporal and spatial scales. Three-dimensional water vapor fields can be retrieved with improved spatial coverage from measurements obtained using a network of scanning microwave radiometers. To investigate this potential, an observation system simulation experiment was performed in which synthetic examples of retrievals using a network of radiometers were compared with results from the Weather Research and Forecasting model at a grid scale of 500 m. These comparisons show that the 3-D water vapor field can be retrieved with an accuracy of better than 15%–20%. A ground-based demonstration network of three compact microwave radiometers was deployed at the Atmospheric Radiation Measurement Southern Great Plains site in Oklahoma. Results using these network measurements demonstrated the first retrieval of the 3-D water vapor field in the troposphere at fine spatial and temporal resolutions.**

***Index Terms*—Atmospheric measurement, electromagnetic tomography, humidity measurement, microwave radiometry, remote sensing, water vapor.**

Manuscript received November 1, 2008; revised May 2, 2009 and August 8, 2009. First published October 21, 2009; current version published October 28, 2009. This work was supported in part by the National Science Foundation under Grant ATM-0456270 to Colorado State University and in part by Ball Aerospace & Technologies Corp. under contracts to Colorado State University.

S. Padmanabhan was with the Microwave Systems Laboratory, Department of Electrical and Computer Engineering, Colorado State University, Fort Collins, CO 80523-1373 USA. She is now with the Jet Propulsion Laboratory, California Institute of Technology, Pasadena, CA 91109 USA (e-mail: sharmila.padmanabhan@jpl.nasa.gov).

S. C. Reising is with the Microwave Systems Laboratory, Department of Electrical and Computer Engineering, Colorado State University, Fort Collins, CO 80523-1373 USA (e-mail: Steven.Reising@ColoState.edu).

J. Vivekanandan is with the Earth Observing Laboratory, National Center for Atmospheric Research, Boulder, CO 80301 USA (e-mail: vivek@ucar.edu).

F. Iturbide-Sanchez was with the Microwave Systems Laboratory, Department of Electrical and Computer Engineering, Colorado State University, Fort Collins, CO 80523-1373 USA. He is now with the I. M. Systems Group, Inc., at the NOAA/NESDIS/Center for Satellite Applications and Research, Camp Springs, MD 20746 USA (e-mail: Flavio.Iturbide@noaa.gov).

Color versions of one or more of the figures in this paper are available online at http://ieeexplore.ieee.org.

Digital Object Identifier 10.1109/TGRS.2009.2031107

I. Introduction

WATER vapor is both the most abundant and the most variable greenhouse gas in the atmosphere. It affects the Earth's radiation budget, energy transfer, cloud formation, and precipitation distribution. Water vapor affects radiation transfer by absorbing both downwelling solar and upwelling longwave radiation. Water vapor also affects energy transfer because the latent heat of vaporization is a principal mechanism for the transport of energy from the equatorial regions to higher latitudes. The energy released when vapor condenses to form clouds is a substantial driver of the dynamics of the atmosphere. This latent heat release modifies the vertical stability of the atmosphere, influencing weather systems and their associated precipitation patterns. Convective storms have been observed to develop in regions of strong and rapidly evolving moisture gradients with spatial variations on submeso γ scales (2–5 km) [1]–[3]. Improving and extending the available techniques of water vapor measurement have been identified as a key research area by the U.S. Weather Research Program [4]. Measurements of water vapor aloft with high time resolution and fine spatial resolution have the potential to improve forecast skill for the initiation of convective storms [4]. Such measurements may be used for assimilation into and validation of numerical weather prediction (NWP) models [5].

Water vapor in the troposphere is highly variable, both temporally and spatially. Vertical profiles of water vapor are typically measured using instrumented weather balloons known as radiosondes. However, radiosondes are launched operationally from U.S. National Weather Service locations separated by an average of 315 km (http://www.ofcm.gov/fmh3/text/chapter1.htm). Radiosondes are not reusable, restricting their launch to twice daily, 0 and 12 UTC, at most stations. Currently, water vapor profiling by commercial radiometers is limited to retrieving vertical water vapor profiles using observations from a single radiometer at a variety of elevation and azimuth angles [6]–[8]. Due to the relatively high cost of currently available microwave radiometers, measurements of the horizontal variability of water vapor aloft at scales smaller than tens of kilometers have not been available.

TABLE I
THREE-DIMENSIONAL WATER VAPOR MEASUREMENT TECHNIQUES

Sensor	Horizontal Resolution (km)	Vertical Resolution (km)	Temporal Resolution (hr)	Frequency Band
GPS Ground Network	50	0.5 -1 Expected	0.5	L-band
Radiosondes	~315 km spacing	0.1-0.5	12	N/A
COSMIC	200-600	0.1 – 0.5	0.5 (2-hr lag)	L-band
AMSU-B	20	2	12	G-band (183 GHz)
Network of CMR-Hs	0.5	0.5-1	0.16-0.25	K-band

Improving quantitative precipitation forecasts is an important and scientifically challenging objective [9]. Improvements are needed in forecasting the location and amount of precipitation, as well as in understanding the underlying mechanisms and processes of convective initiation [10]. Despite their importance to quantitative precipitation forecasting, current observational technologies for measuring water vapor aloft are inadequate, in part due to insufficient sampling.

In addition to these remote sampling considerations, the accuracy of *in situ* measurements has been inadequate. Humidity biases in radiosonde data that often exceed 5% throughout the troposphere have been recently identified and partially corrected [11], [12]. The capacitive polymer hygrometer introduced dry bias errors of 6.8% in RS80 radiosonde data. A humidity sensor boom cover introduced by Vaisala in late 2000 reduced this error to 3.9% [13]. Residual dry bias errors in the current RS92 radiosondes are still larger during the day than at night by 5%–7% [13]. These dry bias errors have a significant impact on long-term climate measurements. When not sufficiently corrected, such biases can change the quantitative and qualitative interpretation of spatial and temporal variations in convective available potential energy and convective inhibition [14].

Table I describes currently available 3-D water vapor measurements. Currently, water vapor density profiles are obtained *in situ* using hygrometers on radiosondes and remotely using lidars [15], [16], ground-based GPS slant-path delay [17], [18], and satellite radio occultation [19], [20], as well as a small number of spaceborne microwave radiometers [21], [22]. *In situ* radiosonde measurements have excellent vertical resolution but are severely limited in temporal and spatial coverages. In addition, each radiosonde takes 45–60 min to ascend from the ground to the tropopause and is typically advected by upper level winds up to several tens of kilometers in horizontal displacement from its launch site. Differential-absorption lidars measure water vapor with resolution that is comparable to that of radiosondes during only clear-sky conditions from a very limited number of sites [23]. Tomographic inversion applied to ground-based measurements of GPS slant path delay is expected to yield 0.5–1-km vertical resolution at 30-min intervals [17], [18], [24]. In contrast, microwave radiometers can provide nearly continuous measurements of weighted path-integrated water vapor and liquid water in the troposphere. Ground-based microwave radiometers perform such measurements with high temporal resolution and in both clear and cloudy conditions. Water vapor products derived from COSMIC (Constellation Observing System for Meteorology, Ionosphere and Climate) and CHAMP (CHAllenging Minisatellite Payload) using the GPS radio occultation technique have vertical resolutions on the order of 100–500 m [19]. However, the horizontal resolution of the retrieved moisture profiles ranges from 200 to 600 km, depending on the magnitude of the path-integrated refractivity. In addition, the accuracy of the path-integrated water vapor retrieval depends strongly on the accuracy of temperature profiles that are available from operational meteorological analyses such as the European Centre for Medium-Range Weather Forecasts [19].

On the other hand, the prediction of convective initiation requires the knowledge of water vapor variations on submeso γ scales (2–5 km) [1]–[3]. Networks of ground-based multifrequency microwave radiometers have the potential to provide improved vertical, horizontal, and temporal resolutions of water vapor fields. Extending our earlier work [25], this paper demonstrates the implementation of tomographic inversion and spatial interpolation techniques to retrieve the 3-D structure of water vapor in the troposphere with fine spatial and temporal resolutions. The need for deployment of multiple microwave radiometers in a remote sensor network motivated a compact sensor design with low mass, low cost, and low power consumption [26].

In this paper, we present a new remote sensing technique to retrieve the 3-D water vapor field with finer spatial resolution than is currently available. This retrieval is achieved by using tomographic inversion of brightness temperatures measured by a ground-based network (ultimately multiple interconnected networks) of compact microwave radiometers scanning in elevation and azimuth. Section II describes the Compact Microwave Radiometer for Humidity Profiling (CMR-H) [26] and the 1-D water vapor profile retrieval from conventional zenith-pointing measurements. This section includes the correction of brightness temperatures for antenna beamwidth and sidelobe errors. Section III focuses on quantifying the spatial scales of water vapor variation through estimation of correlation distances from semivariograms of outputs of fine-resolution NWP models. The resulting spatial information is applied in the retrieval to calculate water vapor densities in unsampled regions using kriging or spatial interpolation techniques. Section IV describes tomographic reconstruction of the 3-D water vapor field from brightness temperature measurements performed by multiple scanning radiometers in a network that view the same atmospheric volumes from multiple perspectives. The network topology used to demonstrate this reconstruction is an equilateral triangle with compact microwave radiometers at each of its vertices. This section describes the forward model and inversion using tomographic reconstruction techniques. To achieve this requires the regularization of the Jacobian matrix, the use of the absorption line shape to retrieve water vapor densities from the water vapor absorption coefficient, and the use of the kriging techniques described in Section III.

In Section V, an observation system simulation experiment (OSSE) is used to determine the expected accuracy of the 3-D water vapor retrieval technique. An appropriate scanning strategy is developed for an equilateral-triangle network with a nearest neighbor distance of 10 km. Section VI describes the first retrieval of the 3-D water vapor field in the troposphere at fine spatial and temporal resolutions from microwave brightness temperature measurements. These measurements were obtained using a three-node ground-based remote sensing network. The network was deployed at the Atmospheric Radiation Measurement (ARM) Southern Great Plains (SGP) site in Billings, OK. Three-dimensional humidity images were obtained at a variety of altitudes using the new remote sensing technique described in Sections IV and V. Finally, Section VII provides conclusions.

II. Field Measurements Using a Single Compact Microwave Radiometer

To obtain high-resolution ground-based measurements of humidity in the troposphere, the Microwave Systems Laboratory at Colorado State University (CSU) has designed, fabricated, tested, and deployed the CMR-H. The design of the CMR-H takes advantage of state-of-the-art monolithic microwave integrated circuit technology and packaging to achieve small size ($24 \times 18 \times 16$ cm^3), light weight (6 kg), and low power consumption (25–50 W, depending on local weather conditions) [26]. External two-point calibration of the CMR-H uses a tipping curve consisting of sky measurements at 1.25, 1.5, 1.75, 2.0, and 2.25 atmospheres to extrapolate to the "cold" calibration reference of the cosmic background temperature of 2.73 K. The "hot" calibration reference is obtained by measuring a microwave absorber whose temperature is measured precisely using an array of temperature sensing elements. The selection of the four CMR-H frequency channels, i.e., 22.12, 22.67, 23.25, and 24.50 GHz, was based on information content studies performed by Solheim *et al.* [27] and Scheve and Swift [28], wherein water vapor density weighting functions were calculated as a function of frequency near the 22.235-GHz water vapor absorption line to determine the ensemble of frequencies with maximum information content for retrieval of the tropospheric water vapor profile. In addition, these studies helped to identify frequency channels which provide no new information, since their weighting functions are merely a linear combination of those at other channels.

A. Field Measurements Using a Single CMR-H

The CMR-H was deployed to perform field measurements at National Center for Atmospheric Research's Mesa Laboratory as part of the Refractivity Experiment For H_2O Research And Collaborative operational Technology Transfer (REFRACTT'06) from June 21 to August 11, 2006 [25], [29]. The scientific goal of REFRACTT'06 was to obtain very high resolution measurements of water vapor variability and transport in the convective boundary layer using a wide variety of observational techniques. A secondary goal was to assess potential improvements in NWP of precipitation due to the availability of enhanced water vapor measurements. The CMR-H performed collocated measurements with a commercially available Radiometrics WVP-1500 five-channel profiling radiometer. Table II provides the specifications of the two radiometers.

TABLE II
Microwave Radiometer Specifications

Parameter	Colorado State CMR-H	Radiometrics WVP-1500
Frequency Channels (GHz)	22.12, 22.67, 23.25 and 24.50	22.235, 23.035, 23.835, 26.235 and 30.000
Sensitivity (K) @ 1-sec integration time	0.2 - 0.3	0.3
3-dB Antenna Beamwidth (°)	3.0 - 4.0	5.0 - 6.0
Calibration	Internal: Noise Diode and Reference Load	Internal: Noise diode
	External: Tipping curve, Microwave absorber at ambient temperature and LN_2	

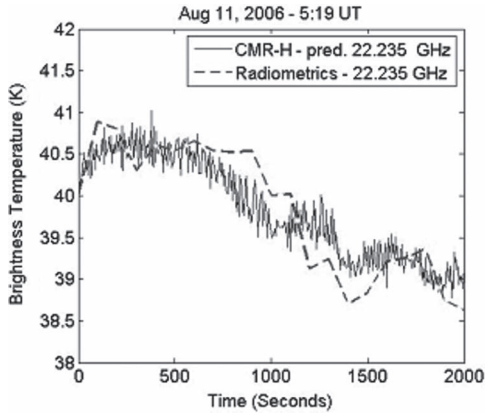

Fig. 1. Comparison of time series of brightness temperatures measured by CMR-H and Radiometrics WVP-1500 five-channel water vapor profiler.

During REFRACTT '06, brightness temperatures were measured by the CMR-H as well as by the Radiometrics WVP-1500 (http://www.radiometrics.com) in the conventional zenith-pointing configuration. Fig. 1 shows a comparison of the time series of brightness temperatures measured by the CMR-H and the Radiometrics WVP-1500 at 22.235 GHz. The brightness temperatures measured at the four CMR-H frequency channels were interpolated to obtain the brightness temperature at 22.235 GHz using the Van-Vleck Weisskopf (VVW) water vapor absorption line shape [30]. Vaisala RS-92 radiosondes were launched from the location of the CMR-H for measurement comparison. The relative humidity accuracy of RS-92 radiosondes is approximately 5% in the lower troposphere and 10% in the middle and upper troposphere [31].

An example of a water vapor density profile retrieved from CMR-H measurements on August 11, 2006 is shown in Fig. 2. Brightness temperatures measured at the four frequencies of CMR-H were used to retrieve the water vapor profile, as described in the next section. Different retrieval techniques were used in retrieving water vapor density profiles from CMR-H and WVR-1500 measurements. Bayesian optimal estimation method was used in retrieving water vapor density from CMR-H measurements, whereas a neural-network-based method was used in the case of WVP-1500 [8]. The profile retrieved from the CMR-H measurements agrees well with

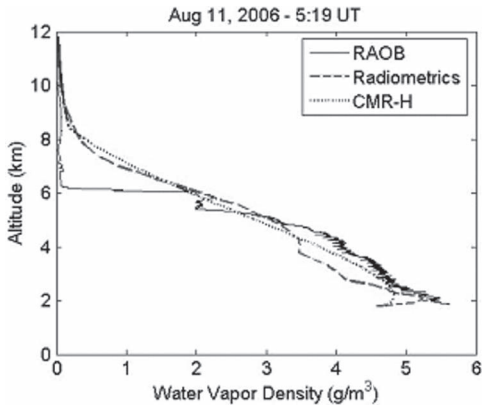

Fig. 2. Comparison of water vapor density profiles measured by radiosonde with those retrieved from microwave brightness temperatures measured by CMR-H and Radiometrics WVP-1500 radiometers.

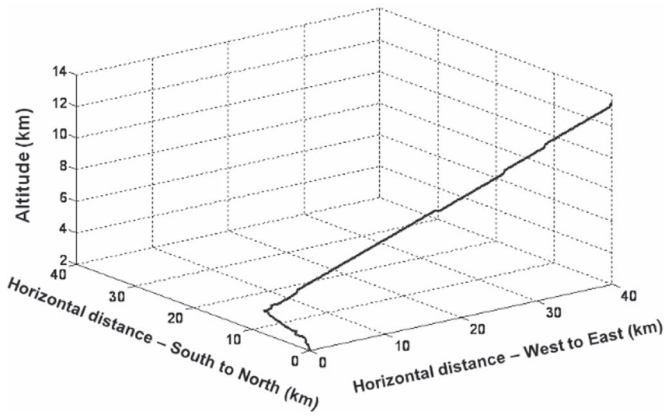

Fig. 3. Trajectory of a radiosonde launched on August 11, 2006.

that retrieved from the WVP-1500 measurements and with that measured by the RS-92 radiosonde. The discrepancy in the profiles at greater than 6-km altitude is thought to be due to the significant advection of the radiosonde horizontally by winds aloft, in addition to a reduced radiometric vertical resolution (500 m) when compared with a radiosonde observation (RAOB) (30 m). Fig. 3 shows the trajectory of the radiosonde, which upper level winds advected 10 km to the north and 40 km to the east from the launch location.

B. Inversion of Single-Radiometer Brightness Temperatures

Retrieval of the water vapor profile from the measured brightness temperatures proceeds as follows. A forward model provides a mapping from a measurement space, in this case the brightness temperatures measured by the radiometer, into a state space, here the tropospheric water vapor density. For this process, the forward model, for a plane-parallel atmosphere without scattering, is generated from the radiative transfer equation, which can be expressed as

$$T_B(f) = \int_a^b W(f,z)g(z)\,dz. \tag{1}$$

In the case of atmospheric brightness temperature measurements from the ground, the integral limits are $a = 0$ and $b = H$, corresponding to the surface and the top of the atmosphere, respectively. The weighting function $W(f,z)$ expresses the fractional contribution of the atmospheric emission at altitude z to the brightness temperature T_B at the frequency f. The function $g(z)$ is the distribution function of an atmospheric parameter. In this case, $g(z) = \rho_\nu(z)$, the water vapor density as a function of altitude z.

Modeling the atmosphere as a set of layers with uniform thickness Δz and expressing (1) in a discrete form, microwave emission from the altitudes between z and $z + \Delta z$ contributes an amount $W(f,z)g(z)\Delta z$ (in kelvins) to the brightness temperature T_B at the frequency f. As a consequence, the total measured brightness temperature at this radiometer frequency will be given by (1). A weighting function for a specific atmospheric parameter represents the change in the measured brightness temperature due to a unit change in that parameter as a function of altitude. The weighting function for the water vapor density $\rho_\nu(z)$ at height z and at the frequency f is defined as [32]

$$W(f,z) = \lim_{\substack{\delta\rho_v \to 0 \\ \delta z \to 0}} \frac{\delta T_B}{\delta\rho_\nu(z)\delta z}. \tag{2}$$

From (2), the weighting function for the water vapor is derived as [33]

$$W_{\rho_v}(f,z) = \frac{\partial\kappa_a(z)}{\partial\rho_v(z)}\left[T(z) - T_B'(f,z)\right]e^{-\tau(0,z;f)} \tag{3}$$

where $\kappa_a(z)$ is the water vapor absorption coefficient at altitude z, $\rho_\nu(z)$ is the water vapor density at altitude z, T_B' is the brightness temperature corrected to account for the effect of nonzero antenna beamwidth, $T(z)$ is the air temperature at altitude z, and τ is the atmospheric opacity. The brightness temperature $T_B(\theta,\phi)$ measured by a radiometer at a specified frequency f, elevation angle θ, and azimuth angle ϕ is a weighted average of background brightness temperatures $T_b(\eta,\xi)$ from all elevation (η) and azimuth directions (ξ) and is given by [30]

$$T_B(\theta,\phi) = \frac{\int_0^{2\pi}\int_0^{\pi} P(\theta,\phi;\eta,\xi)T_b(\eta,\xi)\sin(\eta)\,d\eta\,d\xi}{\int_0^{2\pi}\int_0^{\pi} P(\theta,\phi;\eta,\xi)\sin(\eta)\,d\eta\,d\xi} \tag{4}$$

where $P(\theta,\phi;\eta,\xi)$ is the power pattern of the radiometer antenna. $T_B(\theta,\phi)$, the brightness temperature measured by the radiometer, exceeds the brightness temperature T_b^c that would be measured by an infinitesimally narrow-beam antenna aimed at the boresight of the radiometer antenna. The difference $\delta T_B(\theta) = T_B(\theta,\phi) - T_b^c$ is a function of the antenna beamwidth as well as the amount and distribution of atmospheric water vapor [34]. Assuming the radiometer antenna pattern to be Gaussian, this difference δT_B is

$$\delta T_B(\theta) = \frac{\theta_{1/2}^2}{16\ln 2}(T_{\rm mr} - T_{\rm CMB})e^{(-\tau(\theta))} \times \left[2 + (2-\tau(\theta))\tan^{-2}(\theta)\right]\tau(\theta) \tag{5}$$

where $\theta_{1/2}$ is the half-power (3-dB) beamwidth in radians, $T_{\rm CMB}$ is the cosmic microwave background radiation

(a constant 2.73 K, since galactic radiation is negligible for our purposes above ∼3 GHz), $T_{\rm mr}$ is the mean radiating temperature, given by

$$T_{\rm mr}(\theta) = \frac{\int_0^\infty T(z) e^{-\tau(\theta)}\, d\tau(\theta)}{1 - e^{-\tau(\infty,\theta)}} \tag{6}$$

and $\tau(\theta)$ is the slant path opacity at elevation angle θ given by

$$\tau(\theta) = \int_0^H \kappa(s)\, ds. \tag{7}$$

$T_{\rm mr}$ and $\tau(\theta)$ are calculated using radiosonde profiles for the 1-D case and the reference profile for the 3-D case. After removing the contribution due to nonzero beamwidth, the corrected brightness temperature T'_B used as the input to the 1-D inversion algorithm is given by

$$T'_B = T_B - \delta T_B. \tag{8}$$

For a zenith-pointing measurement, the discrete form of the weighting function W is an $m \times n$ matrix, where m is the number of measured frequency channels and n is the number of altitudes at which the water vapor density is to be retrieved. Since the inversion of the measurements to retrieve geophysical quantities requires finding the inverse of W, the solution is underconstrained if the number of measurements available (m) is smaller than the number of spatial samples (n) of the quantity to be retrieved, which is nearly always the case for microwave radiometry. This problem can be overcome to a certain extent by restricting the class of admissible solutions to a set of physically realizable solutions. In this regard, the Bayesian optimal estimation technique [7], [9], [35] was chosen to retrieve the water vapor density profile using the measured brightness temperatures at the four frequencies of the CMR-H. Bayes' theorem provides a formalism to invert the forward model and calculate an *a posteriori* probability density function (pdf) by updating the prior pdf with a measurement pdf. The water vapor density inversion equation is given by

$$\rho_v = \rho_{v,a} + S_{\rho_{v,a}} W^{\rm T} \left(W S_{\rho_{v,a}} W^{\rm T} + S_{T_B}\right)^{-1} (T'_B - W\rho_{v,a}) \tag{9}$$

where ρ_v is the water vapor density profile, $\rho_{v,a}$ is the *a priori* profile, in this case, the 0 UTC RAOB performed at the Denver/Stapleton weather station (Station ID: 72469), $S_{\rho_{v,a}}$ is the error covariance matrix of the *a priori* water vapor profile, and S_{T_B} is the error covariance matrix for the measured brightness temperatures. The measurement errors of the four radiometric channels are assumed to be statistically independent.

Equation (9) gives a nonunique solution for ρ_v. Therefore, the retrieval is performed by selecting a water vapor profile that minimizes a cost function in the form of [7]

$$J(\rho_v) = \left[T'_B - W\rho_v\right]^{\rm T} S^{-1}_{T'_B} \left[T'_B - W\rho_v\right] + \left[\rho_v - \rho_{v,a}\right]^{\rm T} S^{-1}_{\rho_v} [\rho_v - \rho_{v,a}]. \tag{10}$$

To minimize the cost function numerically, the Gauss–Newton method was used to solve for the water vapor density iteratively as

$$\rho_{v_{i+1}} = \rho_{v,a} + S_{\rho_{v,a}} W_i^{\rm T} \left(W_i S_{\rho_{v,a}} W_i^{\rm T} + S_{T_B}\right)^{-1} \times \left[T'_B - W_i\rho_{v_i} + W_i(\rho_{v_i} - \rho_{v,a})\right] \tag{11}$$

where ρ_{v_i} and $\rho_{v_{i+1}}$ are the water vapor profiles before and after iteration i and W_i is the weighting function matrix for iteration i. W is calculated for each iteration using (3). Equation (11) is a modified version of (9) for computing the iterative solution.

The errors in the *a priori* water vapor density and measured brightness temperatures are modeled as multidimensional zero-mean normal distributions with covariance matrices $S_{\rho_{v,a}}$ and S_{T_B}, respectively. The covariance of the observation vector T'_B (with dimension m) is an $m \times m$ square matrix. The covariance of the *a priori* water vapor density $\rho_{v,a}$ (with dimension n) is an $n \times n$ square matrix. The main diagonal of each covariance matrix contains a set of variances of each variable; the off-diagonal elements contain cross-covariances between each pair of variables. In Bayesian optimal estimation, the *a priori* error covariance matrix provides information about the accuracy of the *a priori* of the retrieved state vector, in this case water vapor density. The error covariance matrix of the *a priori* water vapor density $S_{\rho_{v,a}}$ was constructed based on a first-order Markov process, given by

$$S_{\rho_{v,a}}(x,y) = \sigma_a^2 e^{\left(-|x-y|\frac{\delta z}{h}\right)} \tag{12}$$

where x and y are the row and column indices of the error covariance matrix, respectively, σ_a's are the variances of the *a priori* water vapor densities, h is the length scale, empirically estimated as 6 km, and δz is the altitude spacing. $S_{\rho_{v,a}}$ is an $n \times n$ square matrix. The main diagonal elements of the error covariance matrix S_{T_B} of the measured brightness temperatures describe the uncertainty in the measurements, assumed to be $\sigma^2_{T_B} = (0.5\ {\rm K})^2$. This value was obtained from the standard deviation of a long time series (∼3000 s) of stable sky brightness temperatures measured by CMR-H.

In Section IV, the 1-D retrieval method explained in this section is extended to a 3-D tomographic inversion technique for retrieval of the 3-D water vapor field from brightness temperatures measured by a remote sensor network of CMR-Hs. To accomplish this, it is first necessary to study the spatial variability of water vapor, as described in Section III.

III. Spatial Variability of Tropospheric Water Vapor

Knowledge of the spatial scales of water vapor variability at a variety of altitudes is important to infer the spatial resolution of water vapor measurements required to determine where and when atmospheric conditions are likely to lead to convection based on rapidly evolving moisture gradients. The mesoscale and submesoscale variability of water vapor plays an important role in the understanding of cloud formation and nonlinear processes such as radiative transfer. In the study of Deeter and Evans [1], measurements using NASA's Millimeter-wave Imaging Radiometer during the Tropical Ocean Global

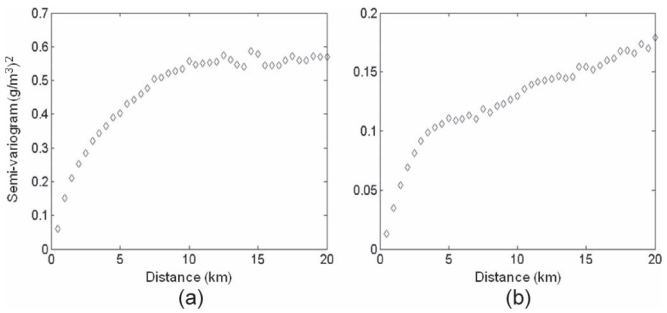

Fig. 4. Semivariograms of water vapor density in WRF model output at (a) 3-km AGL and (b) 5-km AGL at 3:00 UTC.

Atmosphere Coupled Ocean Atmosphere Response Experiment were used to obtain the mesoscale variations of water vapor. An autocorrelation analysis showed that mid-to-upper tropospheric water vapor content varies on submeso γ scales (less than 2–5 km).

The spatial scales of water vapor variability in the troposphere were calculated using outputs of a fine-resolution Weather Research and Forecasting (WRF) model with a 500-m resolution [36]. The WRF model is a next-generation mesoscale and submesoscale NWP system designed for operational forecasting as well as atmospheric science research. It includes a 3-D variational data assimilation system as well as a software architecture that permits computational extensibility. The WRF model is suitable for a broad range of applications on scales ranging from meters to thousands of kilometers. Such applications include research and operational NWP, data assimilation, and parameterized-physics research.

To estimate the spatial correlation statistics of water vapor in the troposphere, a WRF model output with a 500-m grid resolution was used to simulate a cold front and deep convection in northwest Indiana (40.7° N, 86° W) from 2:00 UTC to 3:00 UTC. This model output was also used in the OSSE described in Section V. The spatial correlation statistics of geophysical variables are typically analyzed using spatial autocorrelation functions [37], [38]. A geostatistic used to describe the spatial correlation in the data is the semivariogram, defined as

$$\Gamma(d) = \frac{1}{2m_d} \sum_{1}^{m_d} \left[\rho_v(x_i, y_i) - \rho_v(x_j, y_j)\right]^2 \qquad (13)$$

where m_d is the number of pairs of points in the data set, in this case the WRF model output, at a distance d from each other.

Semivariograms for water vapor densities were calculated from the WRF model output using (13). As shown in Fig. 4, the semivariogram increases as the distance d increases. The slope of the semivariogram is steep for small distances and changes until, at a particular distance, the slope transitions to a minimum relatively constant value for the remainder of the semivariogram. The correlation distance is defined as the distance at which this transition occurs. Various functions have been used to find a best fit to the semivariogram curve [37], [38]. An exponential model (14) was fit to the semivariograms for the WRF model water vapor density outputs at a variety of altitudes to estimate the correlation distances

$$\Gamma(d) = c_0 + c(1 - e^{-d/a}) \qquad (14)$$

where c_0 is the variance at zero distance, c is the sill variance when the distance is maximum, and a is the correlation distance. Semivariograms are different for each altitude level. The semivariogram plots for 3-km and 5-km above ground level (AGL) at 3:00 UTC are shown in Fig. 4. Fig. 5 shows the correlation distances as a function of time at the same two altitudes. The correlation distances and the semivariogram values for the WRF model output were used to calculate the parameters for spatial interpolation, as described in Section IV. Section IV describes the tomographic reconstruction of the 3-D water vapor field from brightness temperature measurements performed by three radiometers in a remote sensor network.

IV. Tomographic Reconstruction of the Tropospheric Water Vapor Field

Retrieval of the 3-D water vapor field from brightness temperature measurements using a network of ground-based radiometers is analytically similar to the fanbeam projection technique commonly used in medical imaging [39]. However, the requirements for performing fanbeam projection with sufficient accuracy are to measure a large number ($\sim$1000) of projections and to measure projections that are uniformly distributed over 180° or 360°. It is not practical to satisfy both of these requirements using a ground-based network of radiometers. However, problems of this type may be more amenable to the use of algebraic reconstruction tomography (ART) techniques [39]. The ART approach to tomographic imaging involves setting up algebraic equations to solve for the unknown targets in terms of the measured projection data. This section describes the formulation of the forward model for the measured brightness temperatures, the inversion of the brightness temperatures to obtain the water vapor absorption coefficients, the ART of the water vapor absorption coefficients, and the retrieval of water vapor using its absorption line shape. Finally, kriging is used to estimate the water vapor at unsampled locations. Kriging, in turn, uses the spatial correlation distances of water vapor density discussed in Section III.

The forward radiative transfer model uses known water vapor densities, either measured or from WRF model outputs, to calculate the expected radiometer brightness temperatures [33], [35], [40] as

$$T_B = T_{\mathrm{CMB}} e^{-\tau(0,z)} + \int_0^z k_{\mathrm{abs}}(z') T(z') e^{-\tau(0,z')}\, dz' \qquad (15)$$

where T_B is the brightness temperature in Kelvin, z is the height of the tropopause in kilometers, k_{abs} is the absorption coefficient at a particular altitude in nepers per kilometer, τ is the optical depth, as defined in Section II-B, and T_{CMB} is the cosmic microwave background radiation. If the scanned domain is divided into M grid cells, the forward model can be expressed in a discrete form as

$$T_{Bi} = T_{\mathrm{CMB}} e^{-\sum_{j=1}^{M} k_{\mathrm{abs\_}j} \Delta r_{ij}} + \sum_{j=1}^{M} k_{\mathrm{abs\_}j} T_j e^{-\tau_{ij}} \Delta r_{ij} \qquad (16)$$

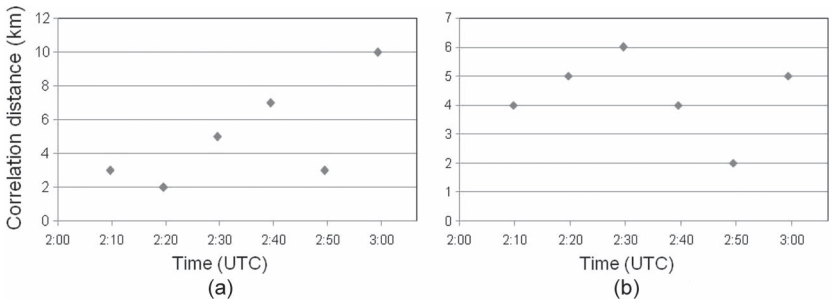

Fig. 5. Time series of water vapor density correlation distance inferred from the semivariograms in Fig. 4 at (a) 3-km AGL and (b) 5-km AGL.

where T_{Bi} is the brightness temperature measured by a radiometer pointing at the ith elevation angle θ_i, $k_{\text{abs\_}j}$ is the absorption coefficient in the jth grid cell, T_j is the air temperature in the jth grid cell, Δr_{ij} is the length of the section of the ray at the ith elevation angle in the jth grid cell, and the opacity τ_{ij} is given as

$$\tau_{ij} = \sum_{m=1}^{j-1} k_{\text{abs\_}m} \Delta r_{im}. \tag{17}$$

We linearize this forward model by replacing the exponential term in (16) with the first two terms of its Taylor series and temporarily ignoring the effect of the cosmic background radiation to obtain

$$T_{Bi} = \sum_{j=1}^{M} k_{\text{abs\_}j} T_j \left(1 - \sum_{l=1}^{j-1} k_{\text{abs\_}l} \Delta r_{il}\right) \Delta r_{ij}. \tag{18}$$

Having formulated the forward model, a reference profile of the pressure, temperature, and water vapor density for a typical atmosphere for the latitude, longitude, and season is used to calculate the brightness temperatures expected to be measured by microwave radiometers for a standard reference atmosphere, called T_{Bref}, for a set of measured elevation angles. For example, the midlatitude summer reference atmospheric profile was used in the OSSE described in Section V. The absorption coefficient in each grid cell was calculated at the CMR-H frequencies using state-of-the-art absorption models [41]–[43]. The variations in the absorption coefficients in each grid cell from their reference values are calculated as

$$\Delta K = K_{\text{abs}} - K_{\text{absref}} \tag{19}$$

and the variations in the calculated brightness temperatures at each elevation angle θ_i from their reference values are

$$\Delta T_B = T_B - T_{\text{Bref}} \tag{20}$$

where K_{abs} and K_{absref} are vectors with elements k_{abs} and k_{absref}, respectively.

In addition, the differencing operation in obtaining ΔT_B significantly reduces any effect of the nonzero antenna beamwidth and sidelobes. For the 3-D water vapor retrieval, the effects of antenna beamwidth and sidelobes on the ΔT_B term are significantly smaller than the measurement uncertainty in the error covariance matrix and hence are neglected. The ΔT_B and ΔK vectors are then related by a Jacobian matrix G as

$$\Delta T_B = G \cdot \Delta K. \tag{21}$$

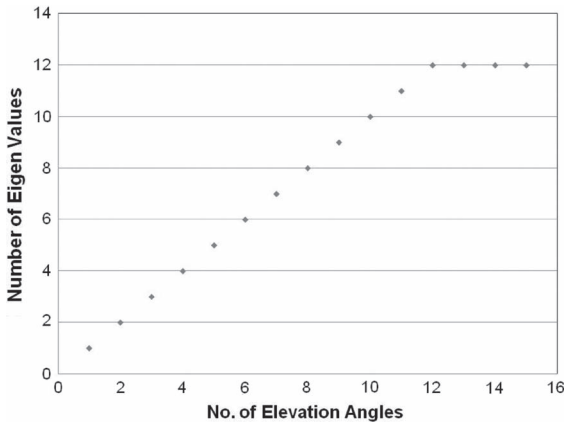

Fig. 6. Number of eigenvalues of the Jacobian matrix versus the number of elevation angles of a scanning microwave radiometer.

Therefore, the elements of the Jacobian matrix G are g_{ij}'s, the partial derivatives of the change in the brightness temperature at the ith elevation angle with respect to the change in absorption coefficient in the jth grid cell, given by

$$g_{ij} = \frac{\partial(\Delta T_{Bi})}{\partial(\Delta K_j)}. \tag{22}$$

The variations in the retrieved absorption coefficients ΔK as a function of measured variations in brightness temperatures ΔT_B are determined as

$$\Delta K = \text{Inv}(G) * \Delta T_B. \tag{23}$$

Since G is not a square matrix, the inverse of G does not exist. We therefore use a regularized inverse of G, as explained hereinafter.

The number of nonzero eigenvalues of G was calculated to find a set of elevation angles with minimum redundancy. The number of eigenvalues is equal to the number of independent ray intersections with unique grid cells. Fig. 6 shows the number of eigenvalues as a function of the number of elevation angles measured by a scanning radiometer. Solving (23) by computing the inverse of the Jacobian matrix G is an ill-posed problem, so no unique solution for ΔK exists. Regularization techniques are needed to solve such ill-posed problems. In this paper, we use the Bayesian optimal estimation method to retrieve ΔK as

$$\Delta K = \Delta K_{a\,priori} + S_{\Delta K_{a\,priori}} G^{\text{T}} (G S_{\Delta K_{a\,priori}} G^{\text{T}} + S_{\Delta T_B})^{-1} \times [\Delta T_B - G \Delta K_{a\,priori}] \tag{24}$$

where $S_{\Delta K_{a\,priori}}$ is the error covariance matrix of the *a priori* absorption coefficients and $S_{\Delta T_B}$ is the error covariance matrix of the measured brightness temperatures.

Given ΔT_B with error statistics $S_{\Delta T_B}$, *a priori* geophysical state vector $\Delta K_{a\,priori}$ with covariance matrix $S_{\Delta K_{a\ priori}}$, and a forward model to calculate the measured ΔT_B in terms of the state vector, the change in the absorption coefficients ΔK is retrieved iteratively by minimizing the cost function (modifying (10) for 3-D retrieval) [7]

$$J(\Delta K) = [T_B - G\Delta K_{a\,priori}]^{\mathrm{T}} S_{T_B}^{-1} [T_B - G\Delta K_{a\,priori}] + [\Delta K - \Delta K_{a\,priori}]^{\mathrm{T}} S_{\Delta K}^{-1} [\Delta K - \Delta K_{a\,priori}]. \tag{25}$$

The Kalman filter technique is used to estimate the water vapor density in each grid cell by performing retrievals in time sequence and ensuring that the retrieved water vapor densities vary smoothly as a function of time. For this method, the previous measurement provides prior information about the water vapor density at the current time. The sequential evolution of the *a priori* measurement is modeled by using a Kalman filter model evolution parameter M_t, given as [35]

$$\Delta K_{a\,priori}(t) = M_t\,(\Delta K_{a\,priori}(t-1)) \tag{26}$$

where M_t operates sequentially in t. Its elements are

$$\frac{\partial \Delta K_{a\,priori}(t-1))}{\partial \Delta K_{a\,priori}(t)}. \tag{27}$$

At time $t-1$, an estimate of $\Delta K_{a\,priori}(t-1)$ is made with an error covariance $S_{\Delta K_{a\,priori}(t-1)}$. The stochastic prediction equation (26) is used to construct an *a priori* estimate $\Delta K_{a\,priori}(t)$ and its covariance $S_{\Delta K_{a\,priori}(t)}$ at time t. These quantities are used in optimal estimation as (24) to provide an updated estimate of the water vapor density. The Jacobian G has elements shown in (22). The Jacobian G and the transition matrix M_t are derived using the WRF model data. For different conditions, G and M_t do need to be updated based on the location. The retrieved absorption coefficients in each WRF model grid cell (0.5 km $\times$ 0.5 km typical horizontal resolution) at the four operating frequencies of CMR-H are then used to compute the water vapor density in the grid cell by performing a nonlinear curve fit to the VVW absorption line shape [30], given as

$$k_{\mathrm{abs\_}j}(f) = (0.3633 \times 10^3) f^2 \rho_{v\_j} \left(\frac{300}{T_j}\right)^{3/2} \gamma \times \left[\left[\left[\left(\frac{1}{T_j}\right)\left(\frac{1}{300}\right)^{3/2}\right] e^{-\frac{644}{T_j}} \times \left[\frac{1}{(22.235-f)^2+\gamma^2} + \frac{1}{(22.235+f)^2+\gamma^2}\right]\right] + 6.6061 \times 10^{-9}\right] \tag{28}$$

where the linewidth parameter γ with units of GHz is

$$\gamma = 2.85 \left(\frac{P_j}{1013}\right)\left(\frac{300}{T_j}\right)^{0.626}\left[1 + 0.018\frac{\rho_{v\_j} T_j}{P_j}\right] \tag{29}$$

where P_j is the pressure, T_j is the temperature, and ρ_{v_j} is the water vapor density in the jth grid cell. The WRF model outputs of pressure and temperature in each grid cell were used in the VVW equation to obtain the curve fits. The water vapor densities in unsampled locations were estimated using spatial interpolation techniques. Kriging provides a solution to the problem of estimation at unsampled grid cells based on a continuous model of stochastic spatial variation [37]. These water vapor densities are calculated using

$$\rho(x_0) = \sum_{i=1}^{N} \lambda_i \rho(x_i) \tag{30}$$

where $\rho(x_0)$ is the water vapor density at location x_0, $\rho(x_i)$'s are the water vapor densities at locations $i = 1, 2, \ldots, N$, and the weights λ_i's are normalized as

$$\sum_{i=1}^{N} \lambda_i = 1. \tag{31}$$

The λ_i's are calculated as

$$\sum_{i=1}^{N} \lambda_i \Gamma(x_i, x_j) + \psi(x_0) = \Gamma(x_j, x_0) \tag{32}$$

where $\Gamma(x_i, x_j)$ is a semivariogram between x_i and x_j, $\psi(x_0)$ is a Lagrange multiplier, and $\Gamma(x_j, x_0)$ is the variogram between x_j and x_0. The Lagrange multiplier is estimated so that it minimizes the mean square error of the variance of the estimated value. The spatial interpolation is performed independently for each altitude using the correlation distance obtained from the WRF model outputs. The correlation distances obtained from the WRF model were averaged over the duration of the simulation.

In summary, the retrieval process consists of using the brightness temperatures measured by the three radiometers to retrieve the water vapor densities in each observed grid cell. These water vapor densities are then used along with correlation distances of water vapor for each altitude to calculate water vapor densities at unsampled locations to yield the 3-D water vapor field with a horizontal resolution of 500 m and a vertical resolution that varies from 0.5 to 1 km (depending on the antenna coverage for different altitudes). The next section describes the measurement configuration and the demonstration of the 3-D retrieval technique via an OSSE using outputs from a fine-resolution WRF NWP model.

V. Expected Performance of a Three-Node Network of Compact Microwave Radiometers

A. Measurement Configuration

To retrieve the 3-D water vapor field with fine spatial and temporal resolutions, we propose a coordinated remote sensor network with a CMR-H at each network node. Each CMR-H,

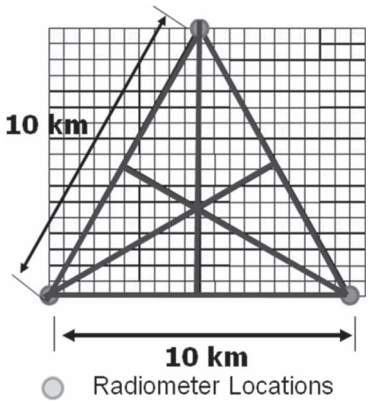

Fig. 7. Equilaterial triangular topology for a three-node scanning radiometer network with a 10-km nearest neighbor distance.

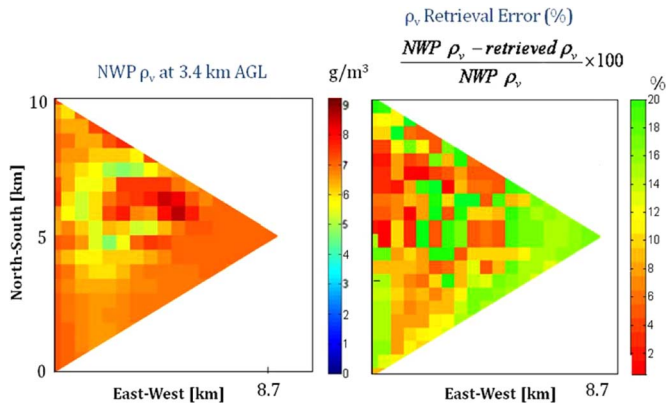

Fig. 8. (a) WRF model output of the water vapor density at 3.4-km AGL over northwest Indiana at 3:00 UTC. (b) Percentage error of the water vapor density retrieved from synthetic brightness temperature measurements also at 3.4-km AGL with WRF model output at 2:00 UTC used as the *a priori*.

mounted atop a precise elevation-over-azimuth positioner, is capable of scanning at a rate of $7^\circ/\mathrm{s}$ in elevation and $25^\circ/\mathrm{s}$ in azimuth. A network of three CMR-Hs in an equilateral triangular configuration with approximately 10-km spacing measures brightness temperatures from which the 3-D water vapor field can be retrieved with a horizontal resolution on submeso γ scales of 500 m, a vertical resolution of 0.5–1 km, and a temporal resolution of 10–15 min, assuming that each radiometer scans the entire hemisphere above and centered on its location.

The elevation-angle scanning pattern was chosen based on an eigenvalue analysis that excludes any angles resulting in redundant grid cell intersections that provide no additional information on the water vapor density. The result is that each radiometer node will scan at 30° spacing in azimuth (12 angles over 360°), and at each azimuth angle, 10 elevation angles are viewed, from zenith to 30° above the horizon. In the case of the triangular network, each node performs multiple scans of the domain in less than 600 s, the shortest decorrelation time of the atmospheric downwelling emission on the spatial scales of these T_B measurements. This decorrelation time is $1/e$ times the maximum autocorrelation of a long (∼3000-s) time series of brightness temperatures measured during REFRACTT'06 for an unstable atmosphere in the presence of rapidly evolving moisture gradients. It provides a maximum duration during which any given radiometer node must complete a scan of its hemispherical coverage volume. If all radiometer nodes in the network complete their volumetric scans within this time period, measurements from all radiometer nodes can be considered to be simultaneous for the purpose of water vapor retrieval.

Fig. 7 shows the optimal topology of a network with three CMR-Hs at the vertices of an equilateral triangle with 10-km nearest neighbor spacing. The line segments represent the azimuth angles viewed by each radiometer using the proposed azimuthal scanning pattern, which was determined using the OSSE described in the next section. Retrievals at each azimuth angle are combined to obtain the retrieved 3-D water vapor field.

B. OSSE

An OSSE was performed in order to evaluate the capability of a network of scanning microwave radiometers to retrieve the 3-D distribution of water vapor in the troposphere. In addition, the results of this OSSE were used to determine the optimal azimuthal scanning strategy for retrieval of the 3-D structure of water vapor with typical spatial and temporal resolutions required to forecast a convective event. To accomplish this, the 3-D water vapor output from a fine-resolution WRF NWP model was compared with retrievals from synthetic brightness temperatures, i.e., those that would have been measured under the same weather conditions by a remote sensor network of three CMR-Hs. The OSSE was performed using the WRF model output for a cold front and deep convection in northwest Indiana (40.7° N, 86° W) from 2:00 UTC to 3:00 UTC. For this OSSE, the *a priori* water vapor field was the WRF model output at 2:00 UTC. Assuming the weather conditions of the WRF model output at 3:00 UTC, the forward radiative transfer model described in Section IV was used to calculate synthetic brightness temperatures at the CMR-H frequencies as a function of azimuth and elevation angles [33].

Next, 3-D moisture fields were retrieved using the algebraic tomographic reconstruction method described in Section IV and compared with the WRF model output. Water vapor densities at the unsampled locations were estimated by using the kriging spatial interpolation technique. This algorithm was based on the spatial characteristics of water vapor densities, including the semivariogram and correlation lengths, as explained in Section III, using the fine-resolution WRF model output.

Fig. 8(a) shows the WRF model output of the water vapor density at 3.4-km AGL at 3:00 UTC. Taking this WRF model output as "truth," the percentage error of the retrieved water vapor density at 3:00 UTC is shown in Fig. 8(b) and calculated as

$$\rho_v \text{ retrieval error } (\%) = \frac{NWP\,\rho_v - retrieved\,\rho_v}{NWP\,\rho_v} \times 100. \quad (33)$$

The OSSE results show that the 3-D water vapor density field can be retrieved with an accuracy of better than 15%–20% at all altitudes. A histogram of the retrieval errors is shown in Fig. 9, demonstrating that the errors in retrieval of water vapor density are roughly uniformly distributed from 5% to 20%. The OSSE retrieval accuracy can be considered to be "worst case" in the sense that the *a priori* field is 1 or 2 h prior to the retrieval; whereas in a real measurement, one can update the *a priori*

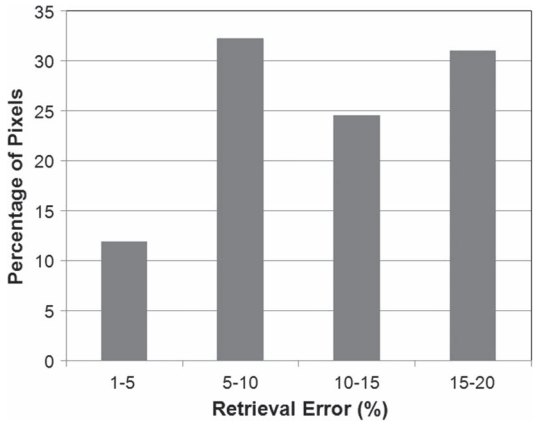

Fig. 9. Histogram of water vapor density retrieval errors in Fig. 8(b) for 3.4-km AGL.

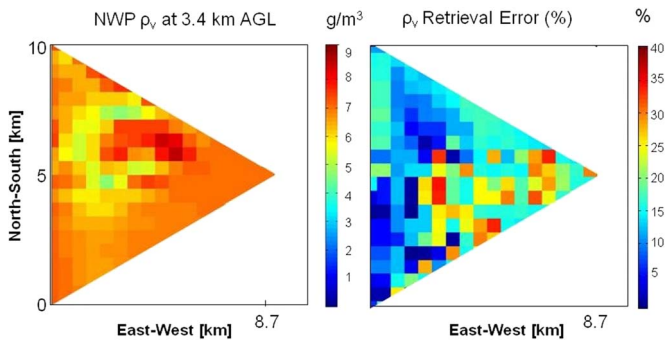

Fig. 10. (a) WRF model output of the water vapor density at 3.4-km AGL over northwest Indiana at 3:00 UTC. (b) Percentage error of the water vapor density retrieved from synthetic brightness temperature measurements also at 3.4-km AGL with WRF model output at 2:00 UTC at the lower left corner of the triangle used as the *a priori*.

estimates every 10 min due to the availability of brightness temperature measurements.

C. Retrieval Sensitivity to a priori

For the retrieval in Fig. 8(b), the *a priori* water vapor density was the output of the fine-resolution WRF model 1 h prior to the retrieval. In order to test the sensitivity of the retrieval algorithm to the quality of the *a priori* estimate, a profile at a single location was instead used to provide a horizontally homogeneous *a priori* water vapor density. This case is analogous to using a radiosonde profile at a single location to provide a homogeneous *a priori* water vapor at each level of the 3-D retrieval. The OSSE was performed using two *a priori* profiles from the following: 1) one vertex of the triangle formed by the radiometer network [0 km east and 0 km north—bottom left corner in Fig. 8(a)] and 2) the median point of the same triangle. Figs. 10 and 11 show the percentage retrieval errors for the 3-D water vapor field retrieved at 3:00 UTC using a vertical profile at one vertex of the triangle at 2:00 UTC and a vertical profile at the median of the triangle at 2:00 UTC, respectively, as the *a priori* profile. As expected, the quality of the retrieval depends on that of the *a priori*. The maximum errors for these retrievals were about 35% for the triangle vertex profile and about 22% for the triangle median point profile. It should be noted that, in both cases for the majority of pixels, the errors are still below

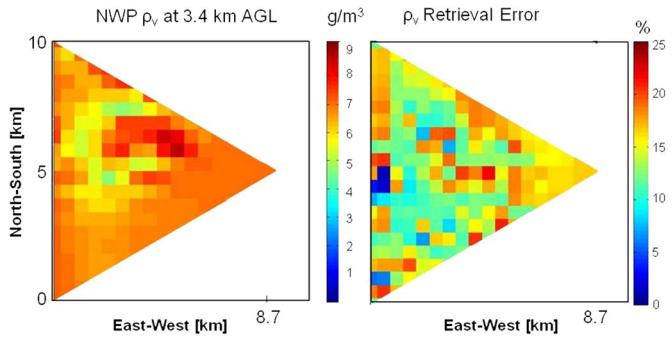

Fig. 11. (a) WRF model output of the water vapor density at 3.4-km AGL over northwest Indiana at 3:00 UTC. (b) Percentage error of the water vapor density retrieved from synthetic brightness temperature measurements also at 3.4-km AGL with WRF model output at 2:00 UTC at the median point of the triangle used as the *a priori*.

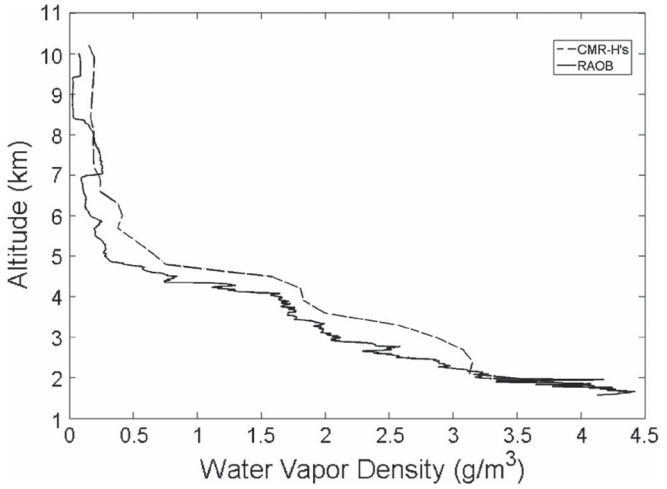

Fig. 12. Comparison of RAOB and CMR-H retrieved water vapor density profile on October 9, 2007.

15%–20%. As expected, the retrieval error using the *a priori* profile from the middle of the triangle was lower than that using the *a priori* profile at one of the vertices.

VI. Field Measurements Using a Three-Node Network of Compact Microwave Radiometers

Two field experiments were performed as a first demonstration of the capability of ART to retrieve the 2-D and 3-D water vapor fields from radiometer network observations with multiple radiometers measuring overlapping atmospheric volumes. In the first field experiment using multiple CMR-Hs to perform scanning measurements, two CMR-H radiometers were deployed at 6-km spacing near Fort Collins, CO, on October 9, 2007. A radiosonde was launched at 6:00 UTC from the CMR-H1 location. Fig. 12 shows a comparison of the water vapor profile measured by the radiosonde and that retrieved from the brightness temperatures measured by the CMR-H1 radiometer. At 8:00 UTC, CMR-H1 and CMR-H2 performed 2-D scanning measurements in the vertical plane containing the two radiometers. The water vapor profile measured by the RAOB launched 2 h earlier was used as the *a priori* water vapor profile to retrieve the 2-D water vapor image using the overlapping scans of the two CMR-Hs. A time series of 2-D water vapor images was retrieved in the region between the two

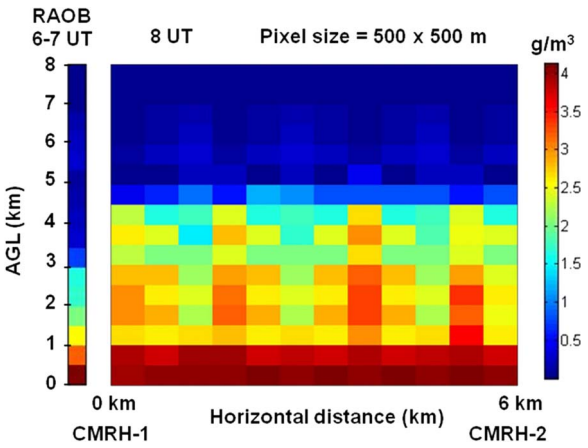

Fig. 13. Two-dimensional water vapor image retrieved in the region between two CMR-H radiometers at 6-km spacing. Each pixel shown has dimensions of 500 m × 500 m.

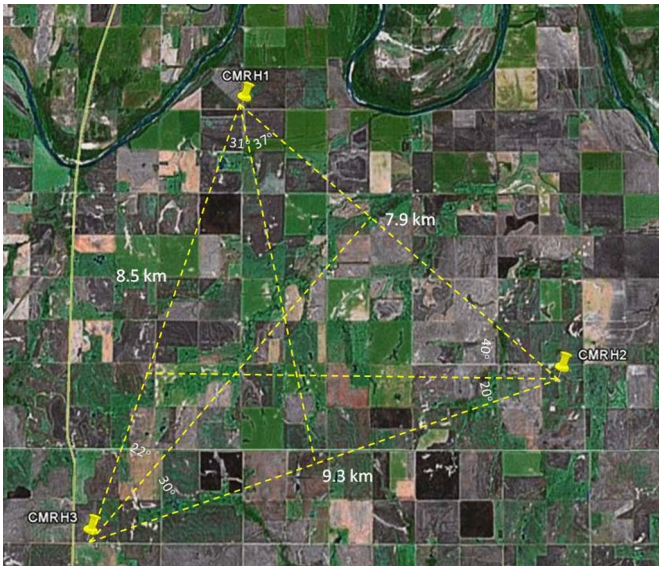

Fig. 14. Map of the demonstration network of three CMR-H radiometers deployed at the ARM-SGP site near Billings, OK. The three azimuth angles scanned by each radiometer are shown as dashed line segments. CMR-H2 was deployed at the ARM-SGP Central Facility.

TABLE III
RADIOMETER DEPLOYMENT LOCATIONS IN OKLAHOMA

Radiometer	Latitude	Longitude	Altitude (m)
CMR-H1	36.6513° N	97.5670° W	305.1
CMR-H2	36.6054° N	97.4857° W	325.2
CMR-H3	36.5782° N	97.5836° W	334.2

radiometers, one example of which is shown in Fig. 13, with a pixel size of 500 m × 500 m.

The second field experiment consisted of measurements using three ground-based microwave radiometers deployed in a roughly equilateral triangle at the ARM-SGP site in Billings, OK, on August 25–31, 2008. The locations of the three radiometers are shown in Fig. 14, in which the CMR-H2 site is located at the ARM-SGP Central Facility. Table III provides the latitudes and longitudes of the three radiometer locations at the ARM-SGP site. A scanning strategy was chosen as described

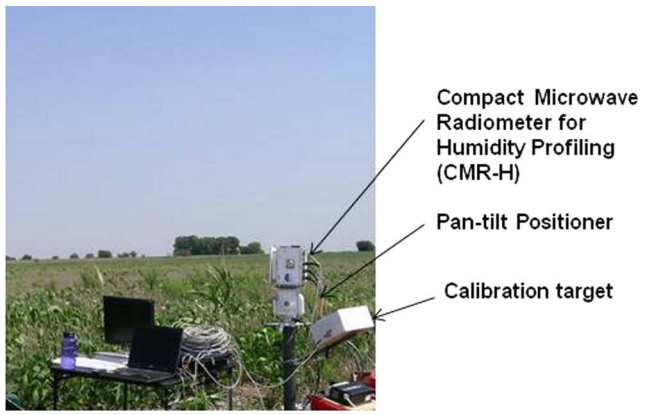

Fig. 15. CMR-H deployed at the ARM-SGP site near Billings, OK, during August 2008.

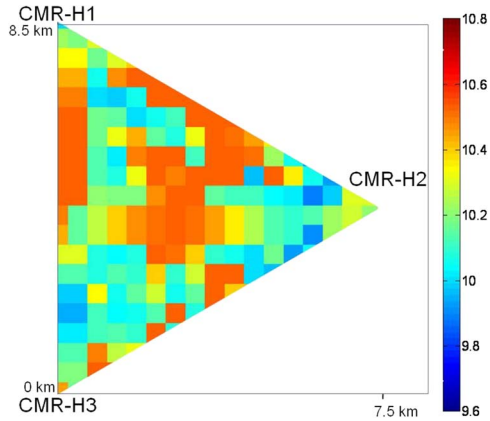

Fig. 16. Image of water vapor density at 2-km AGL in grams per cubic meter near the ARM-SGP Central Facility, retrieved from brightness temperature measurements at 17:30 UTC on August 31, 2008.

in Section V, in which each radiometer scans three angles in azimuth (roughly 30° apart) and 10 angles in elevation from zenith to 30° above the horizon. The azimuthal angles for the three-radiometer network are shown as dashed line segments in Fig. 14. The measured brightness temperatures from each of the three radiometers in the demonstration network were used to retrieve the 3-D water vapor field using algebraic tomographic reconstruction, as described in Section IV.

Fig. 15 shows a CMR-H radiometer, a positioner, and a calibration target deployed at one of the three sites near Billings, OK. Images of retrieved water vapor density at 17:30 UTC on August 31, 2008 at 2-km AGL, 3-km AGL, and 4-km AGL are shown in Figs. 16–18, respectively. The pixel size in each of these images is 500 m × 500 m. The dynamic ranges or horizontal variabilities of water vapor in each of these images are 12%, 13%, and 15%, respectively. The water vapor profile measured by the radiosonde launched at 11:27 UTC was used as the horizontally homogeneous *a priori* for the first retrieval at 16:00 UTC, similar to the cases described in Section V-C. The *a priori* for retrieval of water vapor densities at subsequent times uses Kalman filtering and is updated sequentially from the previous retrieval. These retrieved images clearly demonstrate the capability of a remote sensor network of three CMR-H radiometers to measure the vertical and horizontal variations of water vapor density.

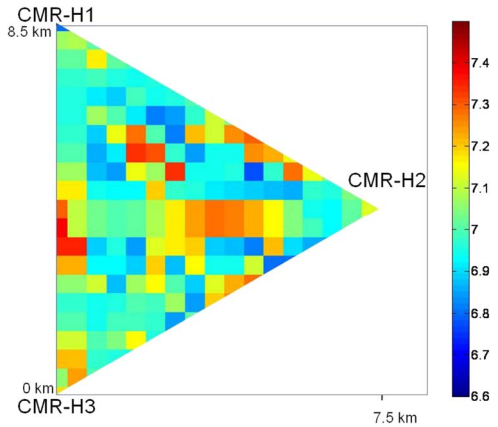

Fig. 17. Image of water vapor density at 3-km AGL in grams per cubic meter near the ARM-SGP Central Facility, retrieved from brightness temperature measurements at 17:30 UTC on August 31, 2008.

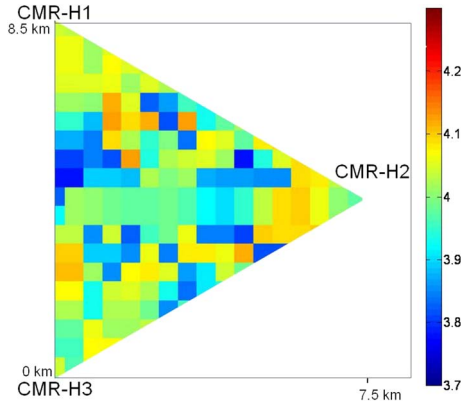

Fig. 18. Image of water vapor density at 4-km AGL in grams per cubic meter near the ARM-SGP Central Facility, retrieved from brightness temperature measurements at 17:30 UTC on August 31, 2008.

VII. Conclusion

Three CMR-Hs have been successfully designed, fabricated, and tested at the Microwave Systems Laboratory at CSU. Each CMR-H is small, light weight, and robust and consumes little power. The low cost of these microwave radiometers enabled the deployment of a sufficient number of scanning microwave radiometers to form a remote sensor network. In such a network, each CMR-H performs a complete volumetric scan, and multiple sensors measure the same atmospheric volumes from different perspectives. The brightness temperatures from multiple scanning compact microwave radiometers were combined to retrieve the 3-D water vapor field. This new retrieval technique combines algebraic tomographic reconstruction, Bayesian optimal estimation, and Kalman filtering to retrieve the 3-D water vapor field as a function of time. An OSSE was performed to demonstrate the retrieval of the 3-D water vapor field and compared with WRF model output with a grid resolution of 0.5 km, yielding a retrieval accuracy of the water vapor density in each individual pixel of better than 15%–20%. The sensitivity of this retrieval technique to the quality of the *a priori* was tested by using a horizontally homogeneous *a priori* profile from model output at a vertex and from model output at the median point of the triangular network.

In order to demonstrate the new 3-D retrieval technique and to obtain high spatial and temporal resolution water vapor fields, a ground-based demonstration network of three radiometers was deployed at the ARM-SGP site in Oklahoma. This network demonstrated the first retrieval of the 3-D water vapor field in the troposphere at fine spatial and temporal resolutions. Complementary measurements from other sensors are needed to perform comparisons and validate retrievals of the 3-D water vapor field obtained from the three-station radiometer network.

Acknowledgment

The authors would like to thank W. Toso (née Foster) and S. Sahoo for their support of the deployment of the three-radiometer network in Oklahoma. The authors would also like to thank Prof. R. Fovell at the University of California, Los Angeles, for generously sharing his WRF model output and the Department of Energy's Atmospheric Radiation Measurement Southern Great Plains site personnel for providing assistance to this project.

References

[1] M. N. Deeter and K. F. Evans, "Mesoscale variations of water vapor inferred from millimeter-wave imaging radiometer during TOGA COARE," *J. Appl. Meteorol.*, vol. 36, no. 2, pp. 183–188, Feb. 1997.

[2] H. Seko, H. Nakamura, Y. Shoji, and T. Iwabuchi, "The meso-γ scale water vapor distribution associated with a thunderstorm calculated from a dense network of GPS receivers," *J. Meteorol. Soc. Jpn.*, vol. 82, no. 1B, pp. 569–586, Mar. 2004.

[3] D. H. Lenschow and B. B. Stankov, "Length scales in the convective boundary layer," *J. Atmos. Sci.*, vol. 43, no. 12, pp. 1198–1209, Jun. 1986.

[4] K. A. Emanuel, D. Raymond, A. Betts, L. Bosart, C. Bretherton, K. Droegemeier, B. Farrell, J. M. Fritsch, R. Houze, M. LeMone, D. Lilly, R. Rotunno, M. Shapiro, R. Smith, and A. Thorpe, "Report of the first prospectus development team of the US weather research program to NOAA and the NSF," *Bull. Amer. Meteorol. Soc.*, vol. 76, no. 8, pp. 1194–1208, Aug. 1995.

[5] Y.-H. Kuo, Y. R. Guo, and E. R. Westwater, "Assimilation of precipitable water measurements into a mesoscale model," *Mon. Weather Rev.*, vol. 121, no. 4, pp. 1215–1238, Apr. 1993.

[6] D. Cimini, T. J. Hewison, L. Martin, J. Güldner, C. Gaffard, and F. S. Marzano, "Temperature and humidity profile retrievals from ground-based microwave radiometers during TUC," *Meteorol. Z.*, vol. 15, no. 5, pp. 45–56, Feb. 2006.

[7] T. J. Hewison, "1D-VAR retrieval of temperature and humidity profiles from a ground-based microwave radiometer," *IEEE Trans. Geosci. Remote Sens.*, vol. 45, no. 7, pp. 2163–2168, Jul. 2007.

[8] K. Knupp, R. Ware, D. Cimini, F. Vandenberghe, J. Vivekanandan, E. Westwater, T. Coleman, and D. Phillips, "Ground-based passive microwave profiling during dynamic weather conditions," *J. Atmos. Ocean. Technol.*, vol. 26, no. 6, pp. 1057–1073, Jun. 2009.

[9] A. Hense, G. Adrian, C. Kottmeier, C. Simmer, and V. Wulfmeyer. (2003). *Quantitative Precipitation Forecast*. [Online]. Available: www.meteo.unibonn.de/projekte/SPPMeteo/reports/SPPLeitAntrag_English.pdf

[10] W. F. Dabberdt and T. W. Schlatter, "Research opportunities from emerging atmospheric observing and modeling capabilities," *Bull. Amer. Meteorol. Soc.*, vol. 77, no. 2, pp. 305–323, Feb. 1996.

[11] F. Guichard, D. Parsons, and E. Miller, "Thermodynamic and radiative impact of the correction of sounding humidity bias in the tropics," *J. Clim.*, vol. 13, no. 20, pp. 3611–3624, Oct. 2000.

[12] D. Turner, B. M. Lesht, S. A. Clough, J. C. Liljegren, H. E. Revercomb, and D. C. Tobin, "Dry bias and variability in Väisälä RS80-H radiosondes: The ARM experience," *J. Atmos. Ocean. Technol.*, vol. 20, no. 1, pp. 117–132, Jan. 2003.

[13] J. Wang and L. Zhang, "Systematic errors in global radiosonde precipitable water data from comparisons with ground-based GPS measurements," *J. Clim.*, vol. 21, no. 10, pp. 2218–2238, May 2008.

[14] T. M. Weckwerth, "The effect of small-scale moisture variability on thunderstorm initiation," *Mon. Weather Rev.*, vol. 128, no. 12, pp. 4017–4030, Dec. 2000.
[15] R. Ferrare, D. Turner, M. Clayton, B. Schmid, J. Redemann, D. Covert, R. Elleman, J. Ogren, E. Andrews, J. E. M. Goldsmith, and H. Jonsson, "Evaluation of daytime measurements of aerosols and water vapor made by an operational Raman lidar over the Southern Great Plains," *J. Geophys. Res.*, vol. 111, no. D5, p. D05 S08, Jan. 2006.
[16] M. Grzeschik, H.-S. Bauer, V. Wulfmeyer, D. Engelbart, U. Wandinger, I. Mattis, D. Althausen, R. Engelmann, M. Tesche, and A. Riede, "Four-dimensional variational analysis of water vapor Raman lidar data and their impact on mesoscale forecasts," *J. Atmos. Ocean. Technol.*, vol. 25, no. 8, pp. 1437–1453, Aug. 2008.
[17] A. Flores, G. Ruffini, and A. Rius, "4D tropospheric tomography using GPS slant wet delays," *Ann. Geophys.*, vol. 18, no. 2, pp. 223–234, Feb. 2000.
[18] A. E. MacDonald, Y. Xie, and R. H. Ware, "Diagnosis of three dimensional water vapor using slant observations from a GPS network," *Mon. Weather Rev.*, vol. 130, no. 2, pp. 386–397, Feb. 2002.
[19] J. Wickert, C. Reigber, G. Beyerle, R. König, C. Marquardt, T. Schmidt, L. Grunwaldt, R. Galas, T. K. Meehan, W. G. Melbourne, and K. Hocke, "Atmosphere sounding by GPS radio occultation: First results from CHAMP," *Geophys. Res. Lett.*, vol. 28, no. 17, pp. 3263–3266, Sep. 2001.
[20] G. Beyerle, T. Schmidt, J. Wickert, S. Heise, M. Rothacher, G. König-Langlo, and K. B. Lauritsen, "Observations and simulations of receiver-induced refractivity biases in GPS radio occultation," *J. Geophys. Res.*, vol. 111, no. D12, p. D12 101, 2006.
[21] A. Somieski, B. Buerki, A. Geiger, H.-G. Kahle, E. C. Pavlis, H. Becker-Ross, S. Florek, and M. Okruss, "Tropospheric water vapor from solar spectrometry and comparison with Jason microwave radiometer measurements," *J. Geophys. Res.*, vol. 111, no. D9, p. D09 104, 2006.
[22] P. W. Rosenkranz, "Retrieval of temperature and moisture profiles from AMSU-A and AMSU-B measurements," *IEEE Trans. Geosci. Remote Sens.*, vol. 39, no. 11, pp. 2429–2435, Nov. 2001.
[23] J. L. Machol, T. Ayers, K. T. Schwenz, K. W. Koenig, R. M. Hardesty, C. J. Senff, M. A. Krainak, J. B. Abshire, H. E. Bravo, and S. P. Sandberg, "Preliminary measurements with an automated compact differential absorption lidar for the profiling of water vapor," *Appl. Opt.*, vol. 43, no. 15, pp. 3110–3121, May 2004.
[24] Y. Xie, J. Braun, A. E. MacDonald, and R. Ware, "Application of GPS slant water vapor tomography to an IHOP storm case with simple constraints," in *Proc. 9th Symp. IOAS-AOLS*, San Diego, CA, 2005.
[25] S. Padmanabhan, S. C. Reising, F. Iturbide-Sanchez, and J. Vivekanandan, "Retrieval of 3-D water vapor field using a network of scanning compact microwave radiometers," in *Proc. IEEE Geosci. Remote Sens. Symp.*, Barcelona, Spain, 2007, pp. 251–254.
[26] F. Iturbide-Sanchez, S. C. Reising, and S. Padmanabhan, "A miniaturized spectrometer radiometer based on MMIC technology for tropospheric water vapor profiling," *IEEE Trans. Geosci. Remote Sens.*, vol. 44, no. 7, pp. 2181–2193, Jul. 2007.
[27] F. Solheim, J. R. Godwin, E. R. Westwater, Y. Han, S. J. Keihm, K. Marsh, and R. Ware, "Radiometric profiling of temperature, water vapor and cloud liquid water using various inversion methods," *Radio Sci.*, vol. 33, no. 2, pp. 393–404, Mar./Apr. 1998.
[28] T. M. Scheve and C. T. Swift, "Profiling atmospheric water vapor with a K-band spectral radiometer," *IEEE Trans. Geosci. Remote Sens.*, vol. 37, no. 3, pp. 1719–1729, May 1999.
[29] R. D. Roberts, F. Fabry, P. C. Kennedy, E. Nelson, J. W. Wilson, N. Rehak, J. Fritz, V. Chandrasekar, J. Braun, J. Sun, S. Ellis, S. Reising, T. Crum, L. Mooney, R. Palmer, T. Weckwerth, and S. Padmanabhan, "REFRACTT-2006: Real-time retrieval of high-resolution, low-level moisture fields from operational NEXRAD and research radars," *Bull. Amer. Meteorol. Soc.*, vol. 89, no. 10, pp. 1535–1548, Oct. 2008.
[30] F. T. Ulaby, R. K. Moore, and A. K. Fung, *Microwave Remote Sensing; Active and Passive*, vol. 1. London, U.K.: Addison-Wesley, 1981.
[31] L. M. Miloshevich, H. Vömel, D. N. Whiteman, B. M. Lesht, F. J. Schmidlin, and F. Russo, "Absolute accuracy of water vapor measurements from six operational radiosonde types launched during AWEX-G and implications for AIRS validation," *J. Geophys. Res.*, vol. 111, no. D9, p. D09 S10, Apr. 2006.
[32] J. A. Schroeder and E. R. Westwater, "Guide to microwave weighting function calculations," U.S. Dept. Commerce, Nat. Ocean. Atmos. Admin., Environ. Res. Labs., Wave Propag. Lab., Boulder, CO, Tech. Memo. ERL WPL–225, Jul. 1992.
[33] M. A. Janssen, "Introduction to passive remote sensing," in *Atmospheric Remote Sensing by Microwave Radiometry*, M. A. Janssen, Ed. New York: Wiley-Interscience, 1993, pp. 1–35.
[34] Y. Han and E. R. Westwater, "Analysis and improvement of tipping calibration for ground-based microwave radiometers," *IEEE Trans. Geosci. Remote Sens.*, vol. 38, no. 3, pp. 1260–1276, May 2000.
[35] C. D. Rodgers, *Inverse Methods for Atmospheric Sounding: Theory and Practice*. Singapore: World Scientific, 2000.
[36] W. C. Skamarock, J. B. Klemp, J. Dudhia, D. O. Gill, D. M. Barker, W. Wang, and J. G. Powers, "A description of the advanced research WRF version 2," Nat. Center Atmos. Res., Boulder, CO, NCAR Technical Notes, 2005.
[37] R. Webster and M. Oliver, *Geostatistics for Environmental Scientists*. London, U.K.: Wiley, 2001.
[38] R. Olea, "A six-step practical approach to semivariogram modeling," *Stoch. Environ. Res. Risk Assess.*, vol. 20, no. 5, pp. 307–318, Jul. 2006.
[39] A. C. Kak and M. Slaney, *Principles of Computerized Tomographic Imaging*. New York: IEEE Press, 1988.
[40] A. V. Bosisio and G. Drufuca, "Retrieval of two-dimensional absorption coefficient structure from a scanning radiometer at 23.8 GHz," *Radio Sci.*, vol. 38, no. 3, p. 8038, Feb. 2003.
[41] P. W. Rosenkranz, "Water vapor microwave continuum absorption: A comparison of measurements and models," *Radio Sci.*, vol. 33, no. 4, pp. 919–928, Jul./Aug. 1998.
[42] P. W. Rosenkranz, "Erratum: 'Water vapor microwave continuum absorption: A comparison of measurements and models'," *Radio Sci.*, vol. 34, no. 4, p. 1025, Jul./Aug. 1999.
[43] J. C. Liljegren, S.-A. Boukabara, K. Cady-Pereira, and S. A. Clough, "The effect of the half-width of the 22-GHz water vapor line on retrievals of temperature and water vapor profiles with a 12-channel microwave radiometer," *IEEE Trans. Geosci. Remote Sens.*, vol. 43, no. 5, pp. 1102–1108, May 2005.

Sharmila Padmanabhan (S'01) received the B.Eng. degree in electronics and telecommunications engineering from the University of Mumbai, Mumbai, India, in 2001, the M.S. degree in electrical and computer engineering from the University of Massachusetts (UMass), Amherst, in 2004, and the Ph.D. degree from Colorado State University (CSU), Fort Collins, in 2009. She was advised by Prof. S. C. Reising, both at UMass and CSU. Her master's research focused on design, testing, calibration, and data analysis for a K-band polarimetric radiometer at the Microwave Remote Sensing Laboratory, UMass. Her Ph.D. research focused on developing algorithms for the tomographic imaging of tropospheric water vapor using a ground-based network of compact microwave radiometers as well as the design, development, characterization, and calibration of compact and low-cost microwave radiometers.

She is currently a Member of the Technical Staff with the Microwave Remote Sensing Instruments section at the Jet Propulsion Laboratory, California Institute of Technology, Pasadena. Her research interests include millimeter- and submillimeter-wave instrumentation for remote sensing, calibration/validation and performance assessment of microwave radiometers, and geophysical retrieval algorithm development.

Dr. Padmanabhan received the Young Scientist Award at the URSI General Assembly in New Delhi, India, in 2005. While at UMass, she received the Second Place in the IEEE Geoscience and Remote Sensing Student Paper Competition at IGARSS 2003 in Toulouse, France. During the fall of 2006, she was an Advanced Study Program Graduate Visitor in the Earth Observing Laboratory of the National Center for Atmospheric Research, Boulder, CO. She was also a finalist in the IEEE Geoscience and Remote Sensing Student Paper Competition at IGARSS 2008 in Boston, MA.

Steven C. Reising (S'88–M'98–SM'04) received the B.S.E.E. (*magna cum laude*) and M.S.E.E. degrees in electrical engineering from Washington University, St. Louis, and the Ph.D. degree in electrical engineering from Stanford University, Stanford, CA, in 1998, where he was supported by a NASA Earth Systems Science Fellowship and advised by Prof. U. S. Inan.

He is currently an Associate Professor of electrical and computer engineering with Colorado State University (CSU), Fort Collins. Shortly before joining the CSU faculty in 2004, he received tenure at the University of Massachusetts, Amherst, where he had been an Assistant Professor of electrical and computer engineering since 1998. At Stanford, his research focused on low-frequency remote sensing of lightning and its energetic coupling to the ionosphere, which produces chemical changes and transient optical emissions. During the summers of 1999, 2000, and 2003, he was a Summer Faculty Fellow with the Remote Sensing Division of the Naval Research Laboratory in Washington, DC. His research interests span a broad range of remote sensing disciplines, including passive microwave and millimeter-wave remote sensing of the oceans, atmosphere, and land; microwave circuits and radiometer systems; lidar systems for sensing of temperature and winds in the middle and upper atmosphere; and atmospheric electrodynamics. He has been a Principal Investigator of ten grants from NSF, NASA, ONR, NRL (subcontract from the NPOESS Integrated Program Office), the University of Rome (subcontract from ESA), and Ball Aerospace & Technologies Corp.

Dr. Reising is the Vice President of Technical Activities of the IEEE Geoscience and Remote Sensing Society (GRSS). He has served as an elected member of the IEEE GRSS Administrative Committee continuously since 2003, after three-year terms as Editor of the GRSS Newsletter (2000–2002) and Associate Editor for University Profiles (1998–2000). He has been an Associate Editor of the IEEE GEOSCIENCE AND REMOTE SENSING LETTERS (GRSL) since its founding in 2004. He was a Guest Editor of the IEEE TRANSACTIONS ON GEOSCIENCE AND REMOTE SENSING (TGARS) for the IGARSS 2008 Special Issue published in November 2009 and the Special Issue on Microwave Radiometry and Remote Sensing Applications published in July 2007. He has served as a Reviewer for TGARS, GRSL, the IEEE TRANSACTIONS ON MICROWAVE THEORY AND TECHNIQUES, the *Journal of Atmospheric* and *Oceanic Technology*, the *Journal of Oceanography*, *Radio Science*, and *Geophysical Research Letters*. In organizing scientific meetings, he was one of two Technical Program Cochairs of the IEEE International Geoscience and Remote Sensing Symposium, IGARSS 2008, in Boston, MA, with over 1700 attendees. He serves as the General Chair of MicroRad'06, the 9th Specialist Meeting on Microwave Radiometry, held in March 2006 in San Juan, Puerto Rico, with 126 attendees from 15 countries. He was the Local Arrangements Chair for IGARSS 2006 in Denver, CO, with over 1250 attendees. He has been an active participant in each IGARSS Technical Program Committee since 2001.

He serves the International Union of Radio Science (URSI) as the Secretary and Chair-Elect (2009–2011) of its United States National Committee (USNC), consisting of ten scientific commissions in applied electromagnetics. Previously, he chaired its annual Student Paper Prize Competition at each National Radio Science Meeting in Boulder, CO from 2004 to 2008 and at the URSI North American Radio Science Meeting in Ottawa in 2007. He chaired the first URSI International Student Paper Prize Competition at the URSI General Assembly in Chicago, IL in August 2008. In addition, he will cochair the Technical Program Committee for the 2010 URSI National Radio Science Meeting to be held in Boulder. He served as a Secretary of USNC-URSI Commission F (2006–2008) and is a member of URSI Commissions F, G, and H, the American Meteorological Society, the American Geophysical Union, Tau Beta Pi, and Eta Kappa Nu. He received the NSF CAREER Award (2003–2008) in the areas of physical and mesoscale dynamic meteorology, and the Office of Naval Research Young Investigator Program Award (2000–2003) for passive microwave remote sensing of the oceans. His Ph.D. student Sharmila Padmanabhan received the Second Prize Student Paper Award at IGARSS 2003 in Toulouse, France, and the URSI Young Scientist Award in New Delhi in 2005. Three of his undergraduate senior design students won two consecutive Best Paper Contests from the IEEE Denver Section and the IEEE Solid-State Circuits Society in 2007 and 2008. He was awarded the Barbara H. and Joseph I. Goldstein Outstanding Junior Faculty Award in 2004, the Lilly Teaching Fellowship for 2001–2002, and a Young Scientist Award at the URSI General Assembly in Toronto, Canada, in 1999. While at Stanford, he received the first place in the USNC/URSI Student Paper Competition at the 1998 National Radio Science Meeting in Boulder.

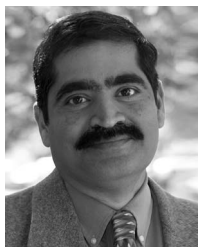

Jothiram Vivekanandan received the Ph.D. degree from Colorado State University, Fort Collins, in 1986.

He holds a Senior Scientist appointment in both the Earth Observing Laboratory and the Research Applications Laboratory. He manages the Remote Sensing Facility at the National Center for Atmospheric Research (NCAR), Boulder, CO. He emphasized the interpretation of remote sensing instruments' responses to clouds and precipitation using mathematical models and actual field observations. He led the development of the dual-wavelength system by adding a millimeter-wave radar to NCAR's S-band polarization radar (S-Pol), and he is currently involved in building an airborne cloud radar. He is an Associate Editor for Radio Science.

Flavio Iturbide-Sanchez (S'03–M'07) received the B.S.E.E degree in electronics engineering from the Autonomous Metropolitan University, Mexico City, Mexico, in 1999, the M.S.E.E. degree in electrical engineering from the Advanced Studies and Research Center of the National Polytechnic Institute, Mexico City, Mexico, in 2001, and the Ph.D. degree from the University of Massachusetts, Amherst, in 2007, where he was advised by Prof. S. C. Reising and supported by the National Science Foundation. His Ph.D. research focused on the miniaturization, development, calibration, and performance assessment of low-cost and power-efficient microwave radiometers for remote sensing applications.

From 2001 to 2005, he was a Research Assistant with the Microwave Remote Sensing Laboratory, University of Massachusetts, where he performed research on the design, development, and characterization of highly integrated multichip modules and microwave circuits for low-noise, low-power consumption, high-gain, and high-stability microwave radiometers. From 2005 to 2007, he was with the Microwave Systems Laboratory, Colorado State University, Fort Collins, focusing on design, testing, deployment, and data analysis of the low-cost and power-efficient Compact Microwave Radiometer for Humidity profiling (CMR-H). Since 2008, he has been with the I. M. Systems Group, Inc., at the NOAA/NESDIS/Center for Satellite Applications and Research, Camp Springs, MD. His research interests include communication systems; microwave radiometry; microwave/millimeter-wave IC design and packaging; RF integrated circuits; system-on-a-chip; active antennas; modeling, analysis, design, and measurement of microwave and millimeter-wave circuits and systems; and atmospheric remote sensing, including retrieval algorithms development.

Dr. Iturbide-Sanchez was a finalist in two IEEE Student Paper Competitions, one at the International Geoscience and Remote Sensing Symposium in Anchorage, AK, September 2004 and one at the International Microwave Symposium in San Francisco, CA, June 2006. He was also awarded the Mexican National Council for Science and Technology (CONACYT) Graduate Fellowship from 1999 to 2004.